



HAL
open science

A methodology for attributing extratropical cyclones to climate change: the case study of storm Alex 2020

Mireia Ginesta, Pascal Yiou, Gabriele Messori, Davide Faranda

► To cite this version:

Mireia Ginesta, Pascal Yiou, Gabriele Messori, Davide Faranda. A methodology for attributing extratropical cyclones to climate change: the case study of storm Alex 2020. 2022. hal-03658139v1

HAL Id: hal-03658139

<https://hal.science/hal-03658139v1>

Preprint submitted on 3 May 2022 (v1), last revised 13 Sep 2022 (v2)

HAL is a multi-disciplinary open access archive for the deposit and dissemination of scientific research documents, whether they are published or not. The documents may come from teaching and research institutions in France or abroad, or from public or private research centers.

L'archive ouverte pluridisciplinaire **HAL**, est destinée au dépôt et à la diffusion de documents scientifiques de niveau recherche, publiés ou non, émanant des établissements d'enseignement et de recherche français ou étrangers, des laboratoires publics ou privés.

1 A methodology for attributing extratropical
2 cyclones to climate change: the case study of
3 storm Alex 2020

4 Mireia Ginesta^{1*}, Pascal Yiou¹, Gabriele Messori^{2,3}
5 and Davide Faranda^{1,4,5}

6 ¹Laboratoire des Sciences du Climat et de l'Environnement,
7 LSCE/IPSL, CEA-CNRS-UVSQ, Université Paris-Saclay,
8 Gif-sur-Yvette, 91191, France.

9 ²Department of Earth Sciences and Centre of Natural Hazards and
10 Disaster Science (CNDS), Uppsala University, Uppsala, Sweden.

11 ³Department of Meteorology and Bolin Centre for Climate
12 Research, Stockholm University, Stockholm, Sweden.

13 ⁴London Mathematical Laboratory, 8 Margravine Gardens
14 London, W6 8RH, London, United Kingdom.

15 ⁵LMD/IPSL, Ecole Normale Supérieure, PSL research University,
16 Paris, France.

17 *Corresponding author(s). E-mail(s):

18 Mireia.Ginesta-Fernandez@lsce.ipsl.fr;

19 Contributing authors: pascal.yiou@lsce.ipsl.fr;

20 gabriele.messori@geo.uu.se; davide.faranda@lsce.ipsl.fr;

21 **Abstract**

22 Extreme event attribution aims at evaluating the impact of climate
23 change on extreme events. In this work, we adapt an attribution method-
24 ology applicable to extratropical cyclones, and test it on storm Alex: an
25 explosive extratropical cyclone that affected Southern France and North-
26 ern Italy at the beginning of October 2020. The methodology specifically
27 combines atmospheric analogues, dynamical systems theory and extreme
28 value theory. We first divide 6-hourly ERA5 data into two periods: a
29 counterfactual period with a weak climate change signal (1950–1985)
30 and a factual period with a strong climate change signal (1985–2021).

31 We then identify the 30 cyclones in each period whose sea-level pressure
32 maps were most similar to Alex's map. We term these *analogues* of Alex.
33 We find that analogues in the factual period are more persistent than
34 in the counterfactual period, which may favour severe impacts result-
35 ing from persistent strong winds and heavy precipitation, as was the
36 case for Alex. This effect is compounded by the doubling in accumulated
37 daily precipitation detected in Northern Italy between the counterfac-
38 tual and factual analogues. In the factual period, the analogues also
39 display deeper cyclones with poleward-shifted backward trajectories. Fur-
40 thermore, we identify a seasonal shift of the analogues, from spring to
41 autumn. Finally, the analogues in the factual world are closer to Alex
42 than in the counterfactual. These changes collectively point to high-
43 impact storms like Alex becoming more common in a changing climate.

44 **Keywords:** Extratropical explosive cyclones, Extreme Event Attribution,
45 Climate Change, Analogues

46 Acknowledgments

47 This work is part of the EU International Training Network (ITN) European
48 weather extremes: drivers, predictability and impacts (EDIPI). This project
49 has received funding from the European Union's Horizon 2020 research and
50 innovation programme under the Marie Skłodowska-Curie grant agreement N°
51 956396. The author wishes to thank F Pons, S Thao and Y Robin for the
52 discussions.

53 1 Introduction

54 Under anthropogenic radiative forcing, the atmosphere is experiencing
55 dynamic and thermodynamic changes (Allan et al, 2021). Understanding and
56 predicting such changes is an essential step in order to evaluate climate-related
57 hazards today and in the future (Pörtner et al, 2022). A major effort in this
58 direction has been obtained with extreme event attribution (EEA) (National
59 Academies of Sciences, Engineering, and Medicine, 2016). EEA is an emerging
60 field that originated in the early 2000s (e.g. Stott et al, 2004) whose objective
61 is to estimate to what extent climate change influences the likelihood, sever-
62 ity or frequency of specific extreme climate events. Extreme event attribution
63 combines statistical analyses and physical understanding (Stott et al, 2016),
64 and has been applied to a broad range of extremes, including droughts, cold
65 spells, heatwaves or extreme rainfall events (e.g. Philip et al, 2018; Cattiaux
66 et al, 2010; Stott et al, 2004; Pall et al, 2011).

67 Some extreme event categories have nonetheless proved more difficult to
68 analyse in an attribution framework than others. An example are extratrop-
69 ical cyclones (ETCs), whose location, frequency and intensity depend on a

70 combination of large-scale, synoptic-scale and smaller dynamic and thermody-
71 namic features. This makes it challenging to both understand recent trends in
72 ETC occurrence and project future ones. In the Northern Hemisphere (NH),
73 the number of ETCs has likely increased in recent decades (Chang and Yau,
74 2016), while there is evidence of a decrease in the number of NH deep cyclones
75 in winter (Neu et al, 2013) and in the number of strong cyclones in summer
76 (Chang et al, 2016). However, there is low confidence for such changes as they
77 are subject to high internal variability and local variations and are sensitive
78 to the data set (Tilinina et al, 2013). According to climate change scenarios,
79 the number of ETC in the storm track regions is projected to decrease glob-
80 ally, while the number of extreme cyclones is likely to increase in NH winter
81 (Priestley and Catto, 2022). As stated in the last IPCC report, the precipita-
82 tion associated to ETCs over the NH (Seneviratne et al, 2021) and the number
83 of ETCs associated with extreme precipitation (Lee et al, 2021) are projected
84 to increase (high confidence). However, there is a less clear response regarding
85 wind speed changes, which are expected to be small and subject to regional
86 variations (Seneviratne et al, 2021).

87 These global or hemispheric-scale changes mask a number of important
88 regional trends. For example, in the North Atlantic, there is evidence of an
89 overall poleward shift of the storm track between 1979 and 2010 (Tilinina
90 et al, 2013). According to Tilinina et al (2013), very deep cyclones (<960 hPa)
91 increased in frequency in the North Atlantic region from 1979 to 1990 in most
92 reanalyses, and declined thereafter. Under anthropogenic radiative forcing,
93 simulations for the Coupled Model Intercomparison Projects of phases 5 and
94 6 (CMIP5 and CMIP6) show a tripolar pattern of the winter North Atlantic
95 storm track response to climate change, with an extension further into Europe
96 and a decrease in storm activity on its northern and southern flanks (Harvey
97 et al, 2020; Zappa et al, 2013; Priestley and Catto, 2022). They also show
98 a weakening of the storm activity over the Mediterranean region. However,
99 according to the last IPCC report (Lee et al, 2021), there is low confidence
100 in regional change projections in the NH and especially in the North Atlantic
101 in winter due to: "large natural internal variability, the competing effects of
102 projected upper- and lower-tropospheric temperature gradient changes, and
103 new evidence of weaknesses in simulating past variations in North Atlantic
104 atmospheric circulation on seasonal-to-decadal timescales".

105 The uncertainty surrounding trends in ETCs highlights the difficulty in
106 attributing their occurrence to climate change. Here, we present an attribu-
107 tion methodology applicable to extratropical cyclones, and test it on storm
108 Alex that occurred in October 2020. Storm Alex was an explosive cyclone
109 that affected France and Italy. We demonstrate that a combination of ana-
110 logue analysis, dynamical systems theory and extreme value theory enables to
111 attribute the characteristics and impacts of a cyclone to the ongoing climatic
112 changes.

113 The paper is organized as follows: section 2 describes the characteristics of
114 Alex. Section 3 provides a detailed description of the data and methods used.

115 It is followed by the presentation of the results in section 4 and a discussion
116 and conclusion in section 5.

117 **2 Alex: a high-impact explosive cyclone**

118 Storm Alex was a powerful explosive cyclone (Sanders and Gyakum, 1980; Neu
119 et al, 2013) that affected south-western Europe in October 2020. It formed
120 as a small perturbation south of Greenland and was named by Météo-France
121 on the 1st of October. Favoured by a very strong jet stream with core speeds
122 of up to 100 m/s, Alex deepened rapidly and experienced explosive cycloge-
123 nesis (Sanders and Gyakum, 1980) between the 1st and the 2nd of October.
124 The cyclone made landfall in Brittany on the night of 1–2 October, with very
125 intense surface winds of up to 140 km/h that caused widespread damage. On
126 the 2nd of October, the cyclone remained stationary over the English chan-
127 nel. Southeasterly winds were induced in southern France and northern Italy,
128 carrying warm, humid air from the Mediterranean and producing extremely
129 heavy rainfall and strong winds. This phenomenon is known as a Mediter-
130 ranean episode (WMO, 2020). On the 3rd of October the cyclone weakened and
131 moved to Normandy. Finally, on the 4th of October, Alex headed northward to
132 England and dissipated during the following days over the North Sea. Figure 1
133 shows Alex’s track, the total accumulated precipitation and the maximum 10m
134 wind gust. The persistence of this storm over the same region resulted in severe
135 impacts, especially in southern France and northern Italy. The area located
136 windward of the Alps received heavy and prolonged orographically-driven rain-
137 fall, leading to numerous record-breaking precipitation amounts registered in
138 the Alpes-Maritimes, Var and Piedmont regions. Piedmont had the highest
139 rainfall since 1951, recording 630 mm in 24h in Sambughetto (European State
140 of the Climate, 2020). Saint-Martin-Vésubie, a village in Alpes-Maritimes,
141 recorded 501 mm of precipitation in 24 hours (Météo France, 2020a), which
142 corresponds to more than three times the climatological October precipita-
143 tion (Météo France, 2020b). Alex caused at least 23 fatalities (10 in France,
144 10 in Italy, 1 in Austria, 1 in Poland and 1 in the Czech Republic), more than
145 10 missing people and an estimated economic loss of about 2.7 billion euros
146 (Météo France, 2021; Riviera 24, 2021; The Watchers, 2020; Aon, 2020).

147 **3 Methodology**

148 We compute flow analogues (Yiou, 2014) to find pattern recurrences of Alex
149 in mean sea-level pressure (SLP), and assess changes in the analogues within
150 the ERA5 reanalysis dataset (Hersbach et al, 2020). We use 6-hourly data
151 from 1950 to 2021, which we split into two 35-year periods of equal length: a
152 factual period, from November 1986 to November 2021, and a counterfactual
153 period, from January 1950 to December 1984. For simplicity, we refer to them
154 as [1985-2021] and [1950-1985], respectively. The latter is meant to represent
155 a climate only weakly affected by anthropogenic emissions, while the former

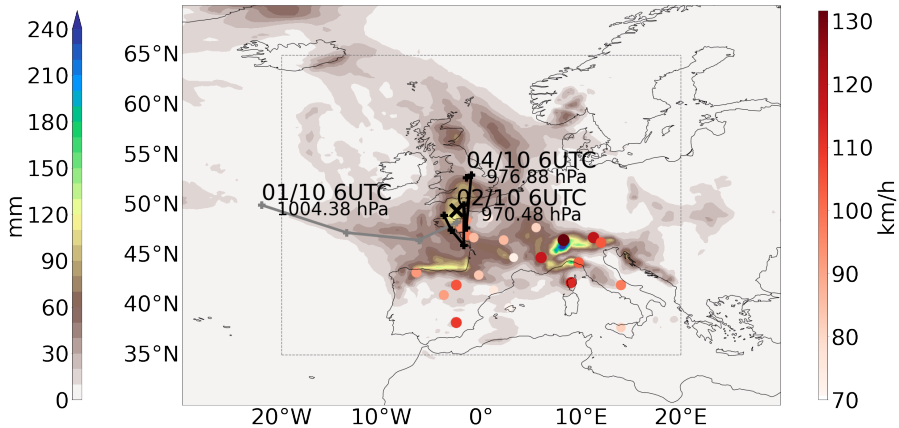


Fig. 1 Backward (grey) and forward (black) trajectories, total accumulated precipitation (shading) and maximum 10m wind gust (coloured dots) between 01/10/2020 at 06:00 UTC and 04/10/2020 at 06:00 UTC. The black cross shows the position of Alex at the time chosen for analysis (02/10/2020 at 06:00UTC). Dashed lines indicate the spatial domain used to find the analogues covering (20W–20E, 35–65N). We use ERA5 6-hourly data to track the cyclone, and ERA5 hourly data to obtain the accumulated precipitation and maximum 10m wind gust (see Section 3 for further details). The maximum 10m wind gust was obtained for every region of France, Italy, and Spain, using spatial masks according to NUTS2 regions (Eurostat, 2021); here we only represent some regions to have a general view of the storm’s passage.

156 presumably displays a stronger anthropogenic influence. We pick 35-year periods as a balance between needing periods that are short enough to assume a
 157 relatively constant anthropogenic radiative forcing, yet long enough to assume
 158 that interannual variability issued from periodic variations such as the El-Niño
 159 – Southern Oscillation averages out. The approach of assuming two periods
 160 around 30-year long is a common assumption in attribution studies (e.g. Luu
 161 et al, 2018; Vautard et al, 2019).
 162

163 3.1 Analogue circulation patterns

164 We identify the 2nd of October 2020 at 6:00UTC as approximately when storm
 165 Alex reached its lowest central pressure while stalling over the English Channel.
 166 We term this time step *lag 0* date of Alex. We then use mean sea-level pressure
 167 over a spatial domain covering (20W–20E, 35–65N) (see also Fig. 1) to identify
 168 the best 30 analogue cyclones in the counterfactual and factual periods. The
 169 choice of 30 analogues is a balance between the needs to have a large enough
 170 sample size to make statistical inferences, and to have analogues that are
 171 suitably close to the reference event we are studying. To select the analogues,
 172 we compute the Euclidean distance between the pressure maps of the 2nd of
 173 October 2020 at 6:00UTC and all other time steps in our dataset. The result is
 174 a time series of Euclidean distances. To avoid counting several times the same
 175 cyclone, we consider a single cyclone in a 7-day window centered on the time
 176 step that has the minimum Euclidean distance. We term this time step *lag 0*

177 date. We chose a 7-day period considering that 3 days is a typical timescale
178 for the formation and decay of an extratropical cyclone (Moon et al, 2021),
179 and that our main purpose is to find individual storms similar to Alex in order
180 to assess changes in their dynamical characteristics.

181 Once we have obtained the *lag 0* dates of the 30 best analogues, we com-
182 pute their composite maps for several variables of interest for each period and
183 the difference map between them. The variables of interest include geopotential
184 height at 500 hPa (Z500), eddy kinetic energy at 500 hPa (EKE500), 24-hour
185 accumulated precipitation (PR), 2m air temperature averaged over 24 hours
186 (T2M), maximum 10m wind gust within 24 hours (WG), and deseasonalized
187 2m air temperature (T2Mdes). EKE500 is computed using a 24-hours differ-
188 ence filter (Wallace et al, 1988). WG is the maximum 3 second wind at 10
189 m height as defined by the World Meteorological Organization (WMO, 1987),
190 where the gust is computed at every time step and the maximum is kept since
191 previous post-processing. To compute PR and WG, we use hourly data, and to
192 evaluate T2M we use 6-hourly data; the start times to compute the accumu-
193 lated values for PR, average values for T2M and maximum values for WG are
194 the *lag 0* dates and end times are 24 hours after them. To evaluate T2Mdes, we
195 first compute a 31-day running-mean smoothed seasonal cycle for each period.
196 We then subtract the smoothed seasonal cycle from the T2M data.

197 We track 48 hours backward and forward cyclone trajectories with a 6-
198 hours time step using a Lagrangian approach, by identifying cyclone centers
199 using minimum mean sea level pressure. Some cyclones emerge from secondary
200 minima of SLP, but they are not detected with this simple method. This dis-
201 advantage is counteracted by individually checking and modifying the cyclone
202 tracking to detect secondary minima, which induces subjectiveness in the
203 method. We have compared factual cyclone tracks with those obtained follow-
204 ing (Pinto et al, 2005), which corresponds to the method M02 from (Neu et al,
205 2013) of the Intercomparison of Mid Latitude Storm Diagnostics (IMILAST),
206 without finding any qualitative differences. Hence, the tracking method used
207 here is not expected to alter the results and conclusions.

208 We count the number of cyclones that experienced explosive cyclogenesis
209 following the definition of Sanders and Gyakum (1980) as those with a Normal-
210 ized Central Pressure Deepening Rate (NDR, Reale et al (2019)) greater than
211 1. We also count the number of cyclones entering the Mediterranean region as
212 those that, after 24 hours or more, are located at latitudes south of 43°N and
213 longitudes east of 3°E.

214 We finally assess the quality of analogues. We first compute *SLP anomalies*
215 by subtracting Alex's SLP from the mean SLP of the analogues in the two
216 periods. Second, we represent the probability distributions of the values of
217 the SLP Euclidean distances between Alex and its analogues and we term it
218 *analogues quality*.

3.2 Dynamical systems metrics

In order to characterise the dynamics of storm Alex and its analogues, we use metrics of local dimension and persistence issued from dynamical systems theory. These metrics can describe the local properties of a dynamical system (Lucarini et al, 2016) and provide information about instantaneous regional atmospheric patterns (e.g. Messori et al, 2017; Alvarez-Castro et al, 2018; Luca et al, 2020).

We follow the approach from Faranda et al (2017) and Lucarini et al (2016), who combine extreme value theory with dynamical systems theory to compute the local dimension d and persistence θ^{-1} of dynamical systems. Local dimension d describes the phase-space geometry of the trajectories in the neighbourhood of a certain state of the system; the higher d , the higher the number of possible evolutions. The persistence θ^{-1} measures the average residence time around a given state, and it is given by the inverse of the extremal index θ . θ has units of frequency (here $1/6$ hours⁻¹, as we use 6-hourly data). Hence, to find the persistence in hours, we multiply θ^{-1} by a factor of 6. A detailed description of the procedure to compute d and θ^{-1} is provided in Appendix A.

3.3 Assessing statistical significance

To assess the statistical significance of the differences between the analogues' averages in the factual and counterfactual periods, we apply a bootstrap procedure with 1000 iterations (Wilks, 2005). Our null hypothesis is that both sets of analogues are drawn from the same, unknown distribution. If the difference of the two original samples — factual minus counterfactual — has an absolute value larger than the 95th percentile of the bootstrap distribution, we reject the null hypothesis and conclude that the differences are statistically significant. To compute Confidence Intervals (CI) for statistical samples we again apply a bootstrap procedure with 1000 iterations, with a 95% confidence level, namely taking the 2.5th and 97.5th percentiles as the lower and upper bounds, respectively. To evaluate the CI of the local dimension d we resample the original sample and compute d in each iteration. To calculate the CI of the extremal index θ we resample the inter-cluster spacings and cluster sizes with equal probabilities (Süveges, 2007), and compute θ in each iteration. Finally, the statistical significance of the differences between boxplots is assessed using a two-sample Kolmogorov-Smirnov test (Wilks, 2005), with a 5% significance level. The null hypothesis is again that both data samples belong to the same, unknown distribution.

4 Results

4.1 Circulation patterns

Figure 2a–c shows the SLP map for the *lag* 0 time step of Alex and the composite SLP for analogues during the counterfactual and factual periods, respectively. Both sets of analogues capture the large-scale structure of Alex,

8 *A methodology for attributing extratropical cyclones to climate change...*

albeit with a weaker magnitude as may be expected by the average of 30 events. Note that when computing the Euclidean distances to find the analogues we use the domain specified in Sect. 3.1 and shown in Fig. 1, and so the North Atlantic large-scale atmospheric configuration might differ between analogues, giving us information about the preferred patterns and dynamic differences of the storms. The difference between the two analogue composites (Fig. 2d) displays an SLP dipole: high pressure anomalies over the North Atlantic and low pressure anomalies over North Africa. This northward (southward) extension of the high (low) pressure system yields an increase in the waviness of the pattern in the factual period. No significant differences are found at the cyclone center. In the middle troposphere (Z500), the analogues capture the low pressure structure over England that characterised Alex (Fig. 2e, f, g). The Z500 differences between the analogues in the two periods (Fig. 2h) partly resemble those in SLP: there is a northward extension and a strengthening of the Azores anticyclone, enhancing the waviness of the pressure field.

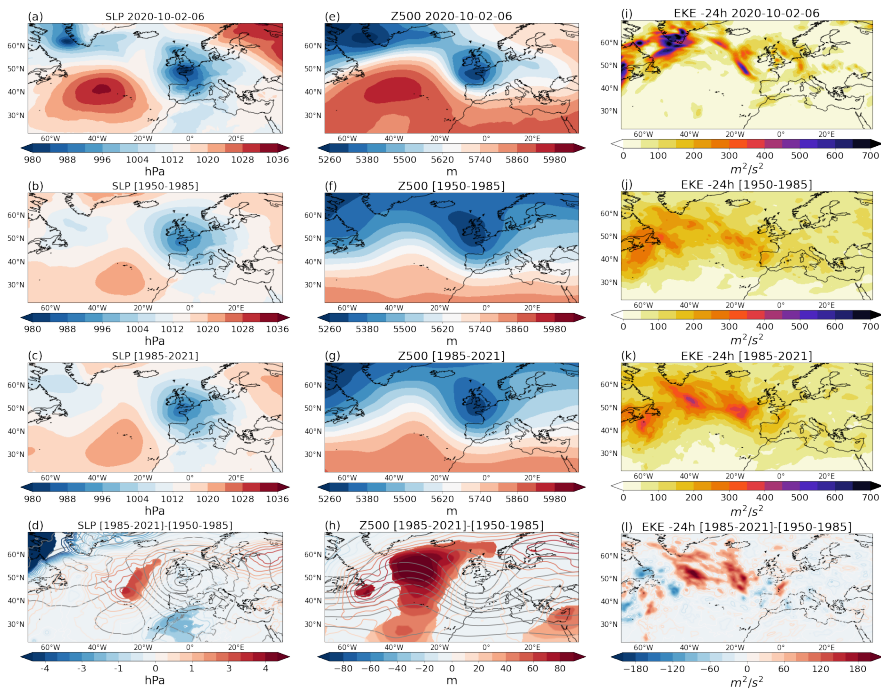


Fig. 2 Mean sea-level pressure (a) and geopotential height at 500hPa (e) at the *lag 0* date of storm Alex and 500 hPa eddy kinetic energy (i) 24 hours prior to the *lag 0*. SLP composites of the 30 analogue storms for the counterfactual (b) and factual (c) periods, and the corresponding Z500 (f,g) and EKE500 (j,k) composites. Factual minus counterfactual differences of SLP (d), Z500 (h) and EKE500 (l). Coloured contours in (d) and (h) show the differences while grey contours show the counterfactual absolute values. Shading in all three panels shows the statistically significant differences.

275 Fig. 3 shows Alex’s SLP and Z500 and the composite SLP and Z500 of
 276 the analogues 12 hours after *lag 0* dates. We found negative anomalies of SLP
 277 over the cyclone region. At upper levels, Z500 depicts high-pressure anomalies
 278 over the North Atlantic. Factual analogue cyclones display a deeper core than
 279 in the counterfactual, and a stronger deepening in the successive 12 hours.
 280 The pattern of the background flow is also wavier in the factual period, due
 281 to low-pressure anomalies in the cyclone region and upstream high-pressure
 282 anomalies.

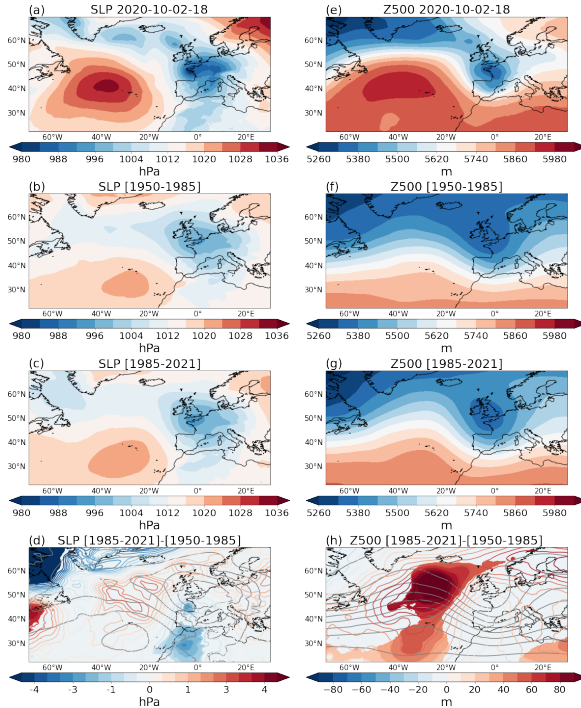


Fig. 3 Same Fig. 2a–h, but for 12 hours after.

283 We further analyse the EKE500 maps and the associated analogues (Figure
 284 2i–l) 24 hours before *lag 0* dates. This field highlights the regions of highest
 285 cyclonic activity previous to the time of the storms. There is a clear differ-
 286 ence between Alex’s EKE500 and that of the analogues in both periods, which
 287 emphasizes that the analogue storms have different origins across the North
 288 Atlantic basin. Composite EKE500 differences (Fig. 2l) show a dipole of posi-
 289 tive anomalies west of England and negative anomalies at lower latitudes,
 290 representing a poleward shift in the factual period with respect to the counter-
 291 factual. In addition, EKE500 differences centered at 48 hours before Alex
 292 show this dipole but shifted about 10° to the west (Fig. B1). This pattern
 293 suggests a higher-latitude origin of the storms in the factual period, consistent

294 with the increase in the waviness found in the SLP maps (Fig. 2d,h). Figure
 295 2l also shows an increase of the maximum EKE500 over most of the North
 296 Atlantic, which implies that storms in the factual period are more energetic
 297 than those in the earlier period.

298 4.2 Cyclone tracking

299 To better assess changes in storm location, the tracks of the analogue cyclones
 300 are shown in Fig. 4. There is a clear latitudinal shift in the backward trajec-
 301 tories: in the factual period (red), the storms head towards Europe from higher
 302 latitudes than those in the counterfactual period (blue). There is no overlap
 303 in the confidence intervals, which means that this shift is statistically significant.
 304 The forward trajectory response is less clear, as most storms dissipate not far
 305 upstream of the English Channel. The backward trajectory of Alex shows that
 306 the cyclone formed and grew at latitudes below 50°N (Fig. 4), indicating a
 307 higher resemblance with those in the counterfactual period.

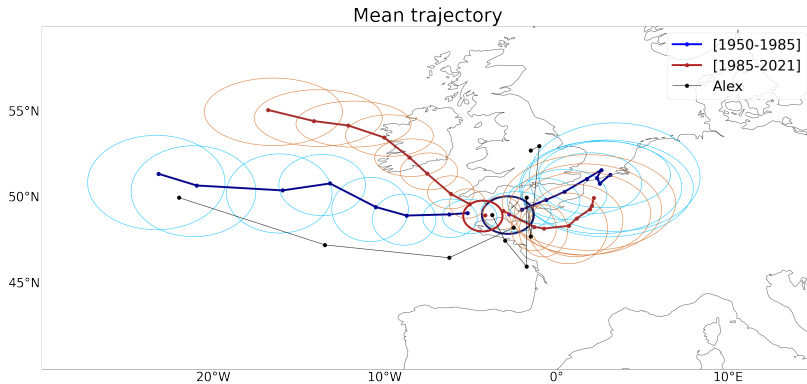


Fig. 4 Alex’s track (black line) and average cyclone tracks for the factual (red thick line) and counterfactual (blue thick line) periods. Dots represent cyclone locations on 6-hourly timesteps. Ellipses show the confidence interval, built using bootstrapping, for each timestep of factual (red thin lines) and counterfactual (blue thin lines): the x-axis shows confidence intervals of longitudes and the y-axis of latitudes. Thick ellipses and dots show the confidence intervals and the average cyclone positions for the dates of the analogues, respectively.

308 A counting of explosive cyclones using the definition of [Sanders and](#)
 309 [Gyakum \(1980\)](#) has been performed for both periods. In the counterfac-
 310 tual period two analogue cyclones underwent explosive cyclogenesis, from
 311 11/03/1976 at 6 AM to 12/03/1976 at 6 PM and from 03/10/1984 at 12 AM
 312 to 04/10/1984 at 12 PM. The latter corresponds to storm Hortense, which
 313 mainly affected Southwestern France ([Météo France, 2019a](#)). In the factual
 314 period, apart from Alex itself only one explosive cyclone has been found, from
 315 04/11/2000 at 12 AM to 05/11/2000 at 18 PM. This cyclone corresponds to
 316 Rebekka, which had its greatest impact in Southern France ([Météo France,](#)
 317 [2019b](#)). The NDRs of the two explosive cyclones in the counterfactual period

318 (1.51 and 1.50, respectively) are larger than that of the single explosive cyclone
 319 in the factual period (1.20). Alex has the largest NDR of our cyclone sample
 320 (1.61). The results presented here only represent a very small fraction of the
 321 North Atlantic cyclones, and the explosive cyclone analogues found take place
 322 over a short period of time, between the 1974 and 2000, which is not enough
 323 to attribute the decline (from 2 explosive cyclones to 1) to climate change as
 324 internal variability could play a higher role. A counting of cyclones that ended
 325 in the Mediterranean region has also been done, and we find 3 in the counter-
 326 factual world and 5 in the factual. This increase in frequency may be linked
 327 to the increase in waviness seen previously, although the results found here
 328 are not enough to draw conclusions on the tendency of the number of cyclones
 329 over the Mediterranean.

330 4.3 Seasonality of analogues

331 Figure 5a,b shows that in the counterfactual period Alex-like storms were more
 332 common in spring while in factual conditions they occur chiefly in autumn.
 333 The number of analogues in winter and summer remains unchanged from
 334 counterfactual to factual periods.

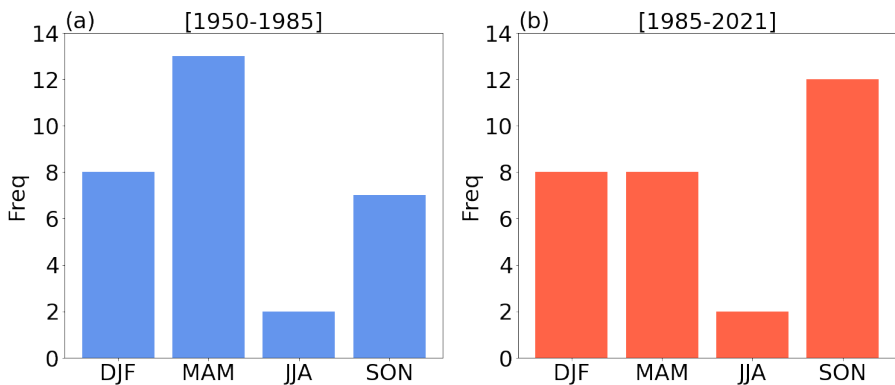


Fig. 5 Frequency of analogues per season, namely winter (DJF), spring (MAM), summer (JJA) and autumn (SON), for the counterfactual (a) and factual (b) periods.

335 The dynamical changes observed in figure 2d,h,l and 4, i.e., a wavier pres-
 336 sure pattern, a strengthening of the eddy activity, and a poleward shift of the
 337 backward trajectories, may be linked to either a direct or an indirect climate
 338 change signal. In the former, climate change would act to shift poleward and
 339 strengthen Alex's analogues directly. In the latter, climate change leads to a
 340 seasonal shift in the occurrence of analogue storms, and the observed changes
 341 correspond to the changes in the mean behavior of the cyclones according to
 342 the season of largest occurrence. Both effects are not exclusive, and changes
 343 may reflect a combination of direct and indirect signals. To help evaluate these

two hypotheses, we search for 30 analogue storms in autumn (September-October-November) and 30 in spring (March-April-May) for each period and repeat the analysis of Sect. 4.1. Z500 field shows a wavier pattern, that is, a northward extension of the high pressure systems, in the factual period during autumn (Fig. B2), while in spring the pattern is less clear (Fig. B3). SLP maps show a deepening of the cyclone over France in autumn, and again a less clear pattern in spring. Hence, we attribute the wavier pattern and the increase in cyclone deepness to (i) a seasonal shift of the analogues from spring to autumn and (ii) changes in autumn pressure patterns, when Alex occurred. This response could be then a combination of (i) an indirect and (ii) a direct climate change signal, even though the proportion of (i) and (ii) is difficult to quantify. The mean tracking shows a clear poleward shift of backward and forward trajectories in spring, while in autumn the shift is weaker (Fig. B4).

4.4 Quality of Analogues

Figure 6a,b shows that composite SLP anomalies over the North Atlantic are smaller in the factual period. Figure 6c shows the distribution of the analogues quality. This distribution shows that the set of factual cyclones provides better analogues than the cyclones from the counterfactual period. We also compute pressure anomalies and analogues quality for spring and autumn analogues (Fig. B5 and B6, respectively). Spring anomalies are larger over the North Atlantic compared to autumn ones in both periods. In the counterfactual period, analogues quality is better in spring than in autumn, which highlights the similarity of Alex with spring storms. In other words, Alex is more similar to analogue cyclones in spring in the counterfactual period, while the North Atlantic atmospheric circulation pattern associated with Alex is closer to that of the autumn analogues, consistent with the pressure field seasonality (Alex occurred in October). However, the quality of autumn analogues improves significantly in the factual world, while in spring there is almost no difference between the counterfactual and factual periods. We thus conclude that Alex was a "black swan" in autumn in the counterfactual period, and rather reflected the characteristics of spring cyclones. However, in the factual period the number of autumn analogues is rising and the quality is improving, consistent with the seasonal shift from spring to autumn seen in figure 5.

4.5 Impacts

In this section, we evaluate three surface fields to detect differences between factual and counterfactual impacts: PR, T2M, WG.

Alex generated heavy precipitation in southern and eastern France and northern Italy (Fig. 7a). The analogues averages (Fig. 7b,c) also show a significant amount of precipitation over this region in both periods, although much lower than storm Alex. There is also much weaker precipitation in southern England, central France and Northern Spain compared to Alex. This may be ascribed to a combination of weaker analogue cyclones and a change in their

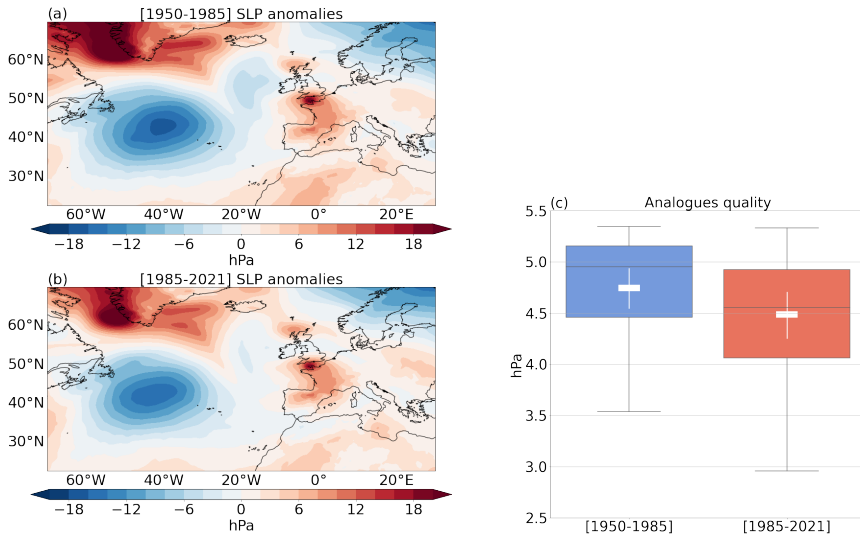


Fig. 6 Sea-level pressure anomalies of counterfactual (a) and factual (b) periods, and analogues quality (c).

386 position that leads to aliasing in the composite. Figure 7d shows a significant
 387 increase in precipitation between the counterfactual and factual analogues of
 388 more than 12 mm in 24 hours windward of the Alps, a region that suffered
 389 catastrophic consequences from Alex.

390 The increase in rainfall is accompanied by a rise in 2m air temperature
 391 (Fig. 7h) leeward of the Alps, probably linked to the foehn effect. In addition,
 392 there is a significant increase in temperature by more than 1.5 K over the
 393 eastern Mediterranean, the northeastern Atlantic Ocean, and the Baltic Sea.
 394 This increase can be due to a direct climate change signal, or it can reflect
 395 a shift in the seasonality of the analogues. To better assess these changes,
 396 we repeated the analysis on the deseasonalized T2M field (Fig. B7). We did
 397 not find significant changes between the counterfactual and factual periods,
 398 meaning that the T2M signal over the Alps and sea regions is mainly due to
 399 a shift in seasonality.

400 Figure 7 (l) shows an increase of the 10m maximum wind gust in the Alps,
 401 Liguria and Provence of up to 5 m/s. Increasing accumulated precipitation
 402 and maximum wind gust imply that factual cyclones are a greater hazard.
 403 10m meridional wind (Fig. B8) shows positive anomalies over the Ligurian
 404 Sea and the Gulf of Venice, which enhances the advection of warm, humid air
 405 from the Mediterranean to Northern Italy and Southeastern France (Fig. B8l).
 406 This increase in meridional wind, related to an increase in the meridional SLP
 407 gradient, can also yield the increase in precipitation seen previously (Fig. 7d,
 408 h).

409 To further quantify the observed increase in precipitation and temperature
 410 in northern Italy and southern France, we first apply a spatial mask (Fig. 7h)
 411 to limit the analysis to the regions of highest impacts for Alex and greater

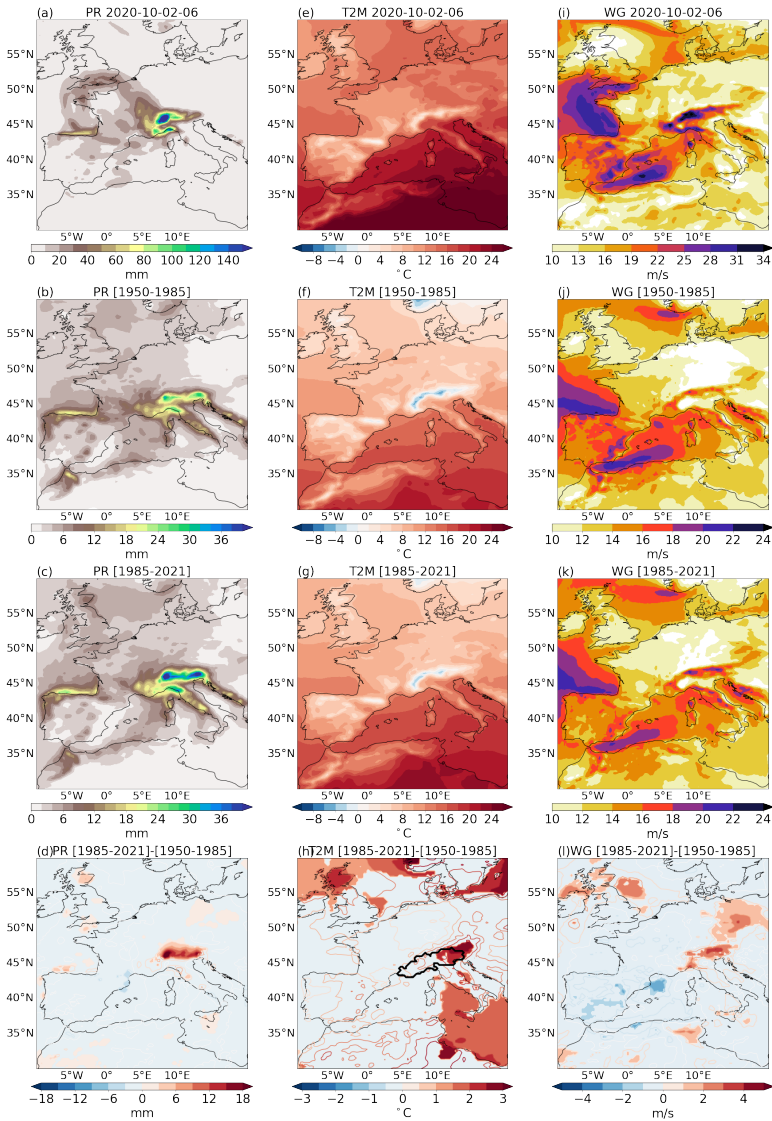


Fig. 7 24-hour accumulated precipitation for Alex (PR, a), counterfactual analogues (b), factual analogues (c), and difference between the two periods (d). Daily average of 6-hourly 2-meter air temperature for Alex (T2M, e), counterfactual analogues (f), factual analogues (g), and difference between the two periods (h). Maximum 10m wind gust within 24 hours for Alex (WG,i), counterfactual analogues (j), factual analogues (k), and difference between the two periods (l). Note that color bars in (a),(i) and (b,c),(j,k) are different. The thick black contour in (h) shows the spatial mask applied in the analysis of Fig. 8 and covers the following regions: Provence-Alpes-Côte d’Azur, Liguria, Piemonte, Lombardia, Valle d’Aoste, Provincia Autonoma di Bolzano, Veneto, Provincia Autonoma di Trento and Friuli-Venezia Giulia.

412 differences between the counterfactual and factual analogues. For Alex's *lag*
 413 0 time step, we compute the 99th quantile of PR, T2M and WG over the
 414 maximum impact region (outlined in Fig. 7h). Then we compute the (spatial)
 415 average values above this quantile in the outlined region. This procedure is also
 416 applied for the analogues. We term the (spatial) averages maximum precipi-
 417 tation (PRmax), maximum temperature (T2Mmax) and maximum wind gust
 418 (WGmax). Hence, we can determine the different probability distributions of
 419 PRmax, T2Mmax and WGmax, linked to an Alex-like storm, in the two sub-
 420 periods (counterfactual and factual) (Fig. 8). We find that PRmax during Alex
 421 is much higher than the rest of the analogues, reaching almost 250 mm. The
 422 medians of PRmax for the analogues are around 50 mm in the counterfactual
 423 period and 80 mm in the factual period. In addition, in the factual period the
 424 75% quantile of the boxplot exceeds 100 mm of rain, while it barely reaches 60
 425 mm in the counterfactual. Hence, in the factual conditions there is an increase
 426 in maximum rainfall. T2Mmax during Alex is higher than that of most of its
 427 analogues. There is also a shift of the T2Mmax distribution towards higher
 428 maximum temperatures in factual conditions by about 2°C. WGmax during
 429 Alex is higher than that of the analogues in factual world but comparable with
 430 the counterfactual maximum. WGmax mean and median values increase from
 431 counterfactual to factual periods by about 2 m/s. PRmax distribution differ-
 432 ences between the two periods are statistically significant, while the T2Mmax
 433 and WGmax differences are not.

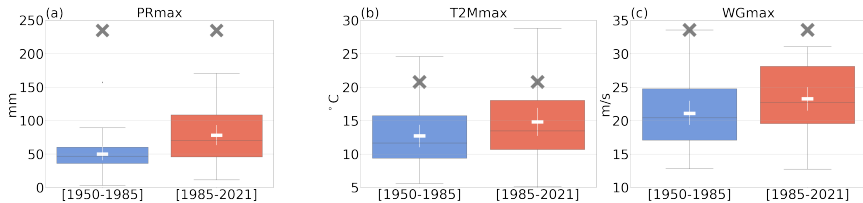


Fig. 8 Boxplot of the area average of the values above the 99% quantile over Southern France and Northern Italy for PR (a), T2M (b) and WG (c). The white horizontal lines show the means of each distribution and the white vertical lines the corresponding confidence intervals. Grey crosses show the values of Alex.

434 4.6 Dynamical system metrics

435 Table 1 shows a decrease in d in the factual world with respect to the coun-
 436 terfactual, which means that the most recent climate is less chaotic than
 437 the counterfactual one. In addition, θ^{-1} shows that factual storms are ~ 4
 438 hours more persistent than in the counterfactual (Fig. 1). Both differences are
 439 statistically significant.

	[1950-1985]	[1985-2021]	Change %
d	7.45 [6.63 8.34]	6.81 [6.05 7.56]	-8.52
θ^{-1}	20.79 [18.90 22.74]	24.06 [21.42 26.82]	15.72

Table 1 Local dimension d and persistence θ^{-1} in hours in the counterfactual (first column) and factual (second column) periods, and the relative change of factual with respect to counterfactual period (third column). Values in brackets show confidence intervals.

5 Discussion and Conclusion

We have presented a methodology for the attribution of extratropical cyclones and their impacts to ongoing climate change. We specifically applied this to storm Alex, which struck southern and western Europe in October 2020. We based our analysis on 30 analogue storms (Yiou, 2014) for Alex in factual (with strong climate change) and counterfactual (with limited climate change) periods from ERA5, and their dynamical properties.

A comparison of the two sets of analogues evidences that the factual storms typically occur on the background of a wavier atmospheric pattern than the counterfactual storms. This stronger meridional component of the flow is linked to a slower-moving pattern (Screen and Simmonds, 2014), as also highlighted by a persistence index we computed using dynamical system theory. This shows an average 4h increase in the persistence of atmospheric patterns in the factual world. Previous studies also found an increase in persistent circulation regimes in recent years (Kornhuber and Tamarin-Brodsky, 2021), and some suggest a possible link with the Arctic Amplification. The observed low-level warming at high latitudes in the NH (Serreze et al, 2009) would act to weaken the zonal wind via the thermal wind relationship, resulting in an increase in amplitude of the polar jet meandering and slower wave propagation, and favouring the longer persistence of weather patters that lead to extreme events. However, due to the complexity of the eddy-mean flow feedbacks, the underlying dynamics are not so clear (Hoskins and Woollings, 2015). In addition, a challenge arises in distinguishing the forced signal from the internal variability (Mann et al, 2017; Barnes and Screen, 2015), partly due to an incomplete knowledge of the influence of high-latitudes to mid-latitude weather as well as a lack of data still remain (Cohen et al, 2014). Hence, according to the last IPCC report, "there is low to medium confidence in the exact role and quantitative effect of historical Arctic warming and sea-ice loss on mid-latitude atmospheric variability" (Doblas-Reyes et al, 2021). Further analysis linking sea-ice loss with the present work's findings could be done, although the lack of reliable sea ice data before 1978 complicates the study.

We further find that, in the factual period, cyclones like Alex are more energetic and become deeper than in the counterfactual. They also tend to occur more frequently in autumn and less frequently in spring. However, this does not seem to influence storm intensity, as both seasons are comparable (Hoskins and Hodges, 2019). When separating analogues according to season, autumn analogues have been found to undergo a large increase in cyclone intensity,

477 which may be related to an increase in humidity leading to a increase in moist
478 baroclinic instability and maximum EKE500 of baroclinic eddies (Gutowski Jr
479 et al, 1992). Sinclair and Watterson (1999) also suggests that an enhancement
480 in water vapor content and a localized increase in baroclinicity could increase
481 regional storm activity. In addition, an increase of the land-sea contrast due
482 to a faster warming over land than over the ocean (Jia et al, 2019) could
483 enhance baroclinicity in summer and early autumn, yielding to an increase
484 of the cyclones intensity. Further investigation using ad hoc numerical model
485 simulations would be required to analyse this and discern the main sources of
486 increased baroclinicity.

487 A poleward shift in the factual period of the eddy activity prior to the
488 storms and of the backward trajectories has been found. According to Hoskins
489 and Hodges (2019), in autumn the main North Atlantic storm track is located
490 farther poleward than in spring. Hence, the poleward shift of the trajectories
491 could be explained by a higher frequency of storms in autumn, as an indirect
492 climate change signal. There is also a weak poleward shift of the backward
493 trajectories in autumn, which acts as a direct climate change signal. However,
494 we have also found that it is in spring when this poleward shift is greater. In
495 addition, the pressure field configuration may act to deflect cyclones poleward
496 over the North Atlantic. We thus deduce that the poleward shift is due to a
497 combination of: (i) a direct climate change that shifts poleward the storms,
498 especially in spring, probably due to a poleward shift of the region of maximum
499 baroclinicity; (ii) an indirect signal, whereby analogues become more common
500 in autumn when the cyclones are located further poleward; and (iii) enhanced
501 low and high pressures patterns that deflect cyclones. Further study must be
502 done to evaluate each components' contribution to the observed poleward shift.

503 Finally, an increase in precipitation in Northern Italy has been detected in
504 the factual period, along with an increase in low-level temperature in the same
505 region and wind gust over the Alps, Liguria and Provence. The increase in
506 precipitation could have a thermodynamic origin, linked to temperature by the
507 Clausius Clapeyron relation, and a dynamic origin, related to the meridional
508 wind and the orographically induced Stau effect. Deseasonalized temperature
509 differences show that the temperature signal corresponds mainly to a seasonal
510 shift of the analogs, which suggests that the increase in precipitation could
511 be related to the shift from spring to autumn cyclones. Hence, in a warmer
512 climate, storms leading to hazards similar to Alex can become more likely, as
513 they occur more in the fall when the Mediterranean is warmer and the air is
514 moister than in spring. The increase in southerly advection by 10m meridional
515 wind has a dynamic origin, as storms become deeper in the factual climate.
516 Southerly winds advect humid air from the Mediterranean, and together with
517 the orographic forcing by the Alps, can increase precipitation. Hence, given
518 the differences observed in the surface fields, more flooding could be triggered
519 at the base of the Alps, the region that suffered the largest impact during the
520 Alex.

521 To summarize, our results show a higher persistence and more persistent
 522 atmospheric pattern for Alex-like cyclones in a warmer climate. Both signals
 523 indicate that the cyclones remain over the same region for longer, favouring
 524 extreme events that result from prolonged weather conditions. There is also
 525 an increase in the maximum eddy kinetic energy and storms become deeper,
 526 especially in autumn, in the factual world. The preferred season for Alex's
 527 analogues shifts from spring to autumn in the factual climate. In addition, in
 528 the factual period, Alex's analogues produce more precipitation in Northern
 529 Italy, and specifically along the southward flank of the Alps, which could trigger
 530 more severe flooding events.

531 The approach used in this work to attribute storm Alex and its impacts to
 532 climate change combines several techniques, including the analogues method
 533 (Yiou, 2014), dynamical systems theory (Faranda et al, 2017), and extreme
 534 event attribution (Stott et al, 2016), to provide a novel, complete toolkit for
 535 attribution studies. This toolkit may be applied with profit to other extra-
 536 tropical and tropical cyclones, and provide new insights on the influence of
 537 climate change on extreme weather phenomena.

538 Statements and declarations

- 539 • Funding: This project has received funding from the European Union's Hori-
 540 zon 2020 research and innovation programme under the Marie Skłodowska-
 541 Curie grant agreement N° 956396.
- 542 • Conflict of interest: The authors declare no conflict of interest.
- 543 • Ethics approval: Not applicable.
- 544 • Consent to participate: Not applicable.
- 545 • Consent for publication: Not applicable.
- 546 • Availability of data and materials: ERA5 data are available on the C3S
 547 Climate Data Store at <https://cds.climate.copernicus.eu/#!/home>.
- 548 • Code availability: The main results of this work were obtained using Python.
 549 The scripts are available upon request.
- 550 • Authors' contributions: MG performed the analysis. MG and DF co-designed
 551 the analyses. All authors participated to the manuscript preparation.

552 References

- 553 Allan RP, Hawkins E, Bellouin N, et al (2021) IPCC, 2021: Summary for Poli-
 554 cymakers. In Climate Change 2021: The physical science basis. Contribution
 555 of Working Group I to the Sixth Assessment Report of the Intergovernmen-
 556 tal Panel on Climate Change [Masson-Delmotte, V., P. Zhai, A. Pirani, S.L.
 557 Connors, C. Péan, S. Berger, N. Caud, Y. Chen, L. Goldfarb, M.I. Gomis, M.
 558 Huang, K. Leitzell, E. Lonnoy, J.B.R. Matthews, T.K. Maycock, T. Water-
 559 field, O. Yelekçi, R. Yu, and B. Zhou (eds.)]. Cambridge University Press.
 560 In Press.

- 561 Alvarez-Castro MC, Faranda D, Yiou P (2018) Atmospheric dynamics lead-
562 ing to West European summer hot temperatures since 1851. Complexity
563 2018:2494,509. <https://doi.org/10.1155/2018/2494509>
- 564 Aon (2020) Global Catastrophe Recap: October 2020. Avail-
565 able at: [http://thoughtleadership.aon.com/documents/20201111_](http://thoughtleadership.aon.com/documents/20201111_analytics-if-october-global-recap.pdf)
566 [analytics-if-october-global-recap.pdf](http://thoughtleadership.aon.com/documents/20201111_analytics-if-october-global-recap.pdf) Accessed: October 2020
- 567 Barnes EA, Screen JA (2015) The impact of arctic warming on the midlatitude
568 jet-stream: Can it? has it? will it? WIREs Clim Change 6:277–286. <https://doi.org/10.1002/wcc.337>
- 570 Cattiaux J, R. Vautard CC, Yiou P, et al (2010) Winter 2010 in Europe:
571 A cold extreme in a warming climate. Geophysical Research Letters 37.
572 <https://doi.org/10.1029/2010GL044613>
- 573 Chang E, Yau A (2016) Northern hemisphere winter storm track trends
574 since 1959 derived from multiple reanalysis datasets. Climate Dynamics
575 47:1435–1454. <https://doi.org/10.1007/s00382-015-2911-8>
- 576 Chang EKM, Ma CG, Zheng C, et al (2016) Observed and projected
577 decrease in northern hemisphere extratropical cyclone activity in summer
578 and its impacts on maximum temperature. Geophysical Research Letters
579 43:2200–2208
- 580 Cohen J, Screen JA, Furtado JC, et al (2014) Recent arctic amplification and
581 extreme mid-latitude weather. Nature Geoscience 7:627–637. <https://doi.org/10.1038/ngeo2234>
- 583 Doblas-Reyes F, Sörensson A, Almazroui M, et al (2021) Linking global to
584 regional climate change. In Climate Change 2021: The physical science basis.
585 Contribution of Working Group I to the Sixth Assessment Report of the
586 Intergovernmental Panel on Climate Change [Masson-Delmotte, V., P. Zhai,
587 A. Pirani, S.L. Connors, C. Péan, S. Berger, N. Caud, Y. Chen, L. Gold-
588 farb, M.I. Gomis, M. Huang, K. Leitzell, E. Lonnoy, J.B.R. Matthews, T.K.
589 Maycock, T. Waterfield, O. Yelekçi, R. Yu, and B. Zhou (eds.)]. Cambridge
590 University Press. In Press.
- 591 European State of the Climate (2020) Storm Alex. Available at [https://](https://climate.copernicus.eu/esotc/2020/storm-alex)
592 climate.copernicus.eu/esotc/2020/storm-alex
- 593 Eurostat (2021) NUTS - Nomenclature of territorial units for statistics. [https://](https://ec.europa.eu/eurostat/web/nuts/background)
594 ec.europa.eu/eurostat/web/nuts/background
- 595 Faranda D, Messori G, Yiou P (2017) Dynamical proxies of North Atlantic
596 predictability and extremes. Scientific Reports [https://doi.org/10.1038/](https://doi.org/10.1038/srep41278)
597 [srep41278](https://doi.org/10.1038/srep41278), URL <https://hal.archives-ouvertes.fr/hal-01340301>

- 598 Freitas ACM, Freitas JM, Todd M (2008) Hitting time statistics and extreme
599 value theory. <https://doi.org/10.48550/ARXIV.0804.2887>
- 600 Gutowski Jr WJ, Branscome LE, Stewart DA (1992) Life cycles of moist
601 baroclinic eddies. *Journal of Atmospheric Sciences* 49:306–319
- 602 Harvey BJ, Cook P, Shaffrey L, et al (2020) The response of the Northern
603 Hemisphere storm tracks and jet streams to climate change in the CMIP3,
604 CMIP5, and CMIP6 climate models. *Journal of Geophysical Research:*
605 *Atmospheres* 125. <https://doi.org/https://doi.org/10.1029/2020JD032701>
- 606 Hersbach H, Bell B, Berrisford P, et al (2020) The ERA5 global reanalysis.
607 *Quat J Roy Met Soc* 146(730):1999–2049. [https://doi.org/https://doi.org/](https://doi.org/https://doi.org/10.1002/qj.3803)
608 [10.1002/qj.3803](https://doi.org/https://doi.org/10.1002/qj.3803), iISBN: 0035-9009 Publisher: Wiley Online Library
- 609 Hoskins B, Woollings T (2015) Persistent extratropical regimes and cli-
610 mate extremes. *Curr Clim Change Rep* 1:115–124. [https://doi.org/10.1007/](https://doi.org/10.1007/s40641-015-0020-8)
611 [s40641-015-0020-8](https://doi.org/10.1007/s40641-015-0020-8)
- 612 Hoskins BJ, Hodges KI (2019) The annual cycle of Northern Hemisphere storm
613 tracks. Part II: Regional detail. *Journal of Climate* 32:1761–1775. <https://doi.org/http://dx.doi.org/10.1175/jcli-d-17-0871.1>
614 [/https://doi.org/http://dx.doi.org/10.1175/jcli-d-17-0871.1](https://doi.org/http://dx.doi.org/10.1175/jcli-d-17-0871.1)
- 615 Jia G, Shevliakova E, Artaxo P, et al (2019) Land–climate interactions. In:
616 *Climate Change and Land: an IPCC special report on climate change, deser-*
617 *tification, land degradation, sustainable land management, food security,*
618 *and greenhouse gas fluxes in terrestrial ecosystems* [P.R. Shukla, J. Skea, E.
619 Calvo Buendia, V. Masson-Delmotte, H.-O. Pörtner, D.C. Roberts, P. Zhai,
620 R. Slade, S. Connors, R. van Diemen, M. Ferrat, E. Haughey, S. Luz, S.
621 Neogi, M. Pathak, J. Petzold, j. portugal pereira, P. Vyas, E. Huntley, K.
622 Kissick, M. Belkacemi, J. Malley, (eds.)]. In press.
- 623 Kornhuber K, Tamarin-Brodsky T (2021) Future Changes in Northern Hemi-
624 sphere Summer Weather Persistence Linked to Projected Arctic Warming.
625 *Geophysical Research Letters* 48. [https://doi.org/https://doi.org/10.1029/](https://doi.org/https://doi.org/10.1029/2020GL091603)
626 [2020GL091603](https://doi.org/https://doi.org/10.1029/2020GL091603)
- 627 Lee JY, Marotzke J, Bala G, et al (2021) Future global climate: Scenario-
628 based projections and near-term information. In *Climate Change 2021:*
629 *The physical science basis. Contribution of Working Group I to the Sixth*
630 *Assessment Report of the Intergovernmental Panel on Climate Change*
631 [Masson-Delmotte, V., P. Zhai, A. Pirani, S.L. Connors, C. Péan, S. Berger,
632 N. Caud, Y. Chen, L. Goldfarb, M.I. Gomis, M. Huang, K. Leitzell, E. Lon-
633 noy, J.B.R. Matthews, T.K. Maycock, T. Waterfield, O. Yelekçi, R. Yu, and
634 B. Zhou (eds.)]. Cambridge University Press. In Press

- 635 Luca PD, Messori G, Pons FME, et al (2020) Dynamical systems theory sheds
636 new light on compound climate extremes in Europe and Eastern North
637 America. *Quarterly Journal of the Royal Meteorological Society* 146:1636–
638 1650. <https://doi.org/https://doi.org/10.1002/qj.3757>
- 639 Lucarini V, Faranda D, Wouters J (2012) Universal Behaviour of Extreme
640 Value Statistics for Selected Observables of Dynamical Systems. [https://
641 doi.org/10.1007/s10955-012-0468-z](https://doi.org/10.1007/s10955-012-0468-z)
- 642 Lucarini V, Faranda D, Freitas ACM, et al (2016) Extremes and recurrence in
643 dynamical systems. [https://doi.org/https://doi.org/10.48550/arXiv.1605.
644 07006, 1605.07006](https://doi.org/https://doi.org/10.48550/arXiv.1605.07006)
- 645 Luu LN, Vautard R, Yiou P, et al (2018) Attribution of extreme rainfall events
646 in the South of France using EURO-CORDEX simulations. *Geophysical
647 Research Letters* 45:6242–6250. [https://doi.org/https://doi.org/10.1029/
648 2018GL077807](https://doi.org/https://doi.org/10.1029/2018GL077807)
- 649 Mann ME, Rahmstorf S, Kornhuber K, et al (2017) Influence of anthropogenic
650 climate change on planetary wave resonance and extreme weather events.
651 *Scientific Reports* 7. <https://doi.org/10.1038/srep45242>
- 652 Messori G, Caballero R, Faranda D (2017) A dynamical systems approach
653 to studying midlatitude weather extremes. *Geophysical Research Letters*
654 44:3346–3354. <https://doi.org/https://doi.org/10.1002/2017GL072879>
- 655 Moon W, Manucharyan GE, Dijkstra HA (2021) Baroclinic instability and
656 large-scale wave propagation in a planetary-scale atmosphere. [https://doi.
657 org/https://doi.org/10.1002/qj.4232](https://doi.org/https://doi.org/10.1002/qj.4232)
- 658 Météo France (2019a) Tempête Hortense du 4 octobre 1984. Available at [http:
659 //tempetes.meteofrance.fr/IMG/anthemis_pdf/19841004.pdf](http://tempetes.meteofrance.fr/IMG/anthemis_pdf/19841004.pdf)
- 660 Météo France (2019b) Tempête Rebekka du 6 novembre 2000. Available at
661 http://tempetes.meteo.fr/IMG/anthemis_pdf/20001106.pdf
- 662 Météo France (2020a) Bulletin climatique octobre 2020. Available at
663 [https://donneespubliques.meteofrance.fr/donnees_libres/bulletins/BCM/
664 202010.pdf](https://donneespubliques.meteofrance.fr/donnees_libres/bulletins/BCM/202010.pdf)
- 665 Météo France (2020b) Tempête Alex: des intempéries exceptionnelles.
666 Available at [https://meteofrance.com/actualites-et-dossiers/climat/
667 tempete-alex-des-intemperies-exceptionnelles](https://meteofrance.com/actualites-et-dossiers/climat/tempete-alex-des-intemperies-exceptionnelles)
- 668 Météo France (2021) Tempête Alex du 2 octobre 2020. Available at [http:
669 //tempetes.meteo.fr/IMG/anthemis_pdf/20201002.pdf](http://tempetes.meteo.fr/IMG/anthemis_pdf/20201002.pdf)

670 National Academies of Sciences, Engineering, and Medicine (2016)
 671 Attribution of Extreme Weather Events in the Context of Climate
 672 Change. The National Academies Press, Washington, DC, <https://doi.org/10.17226/21852>, URL [https://www.nap.edu/catalog/21852/
 673 //doi.org/10.17226/21852](https://www.nap.edu/catalog/21852/attribution-of-extreme-weather-events-in-the-context-of-climate-change), URL [https://www.nap.edu/catalog/21852/
 attribution-of-extreme-weather-events-in-the-context-of-climate-change](https://www.nap.edu/catalog/21852/

 674 attribution-of-extreme-weather-events-in-the-context-of-climate-change)

675 Neu U, Akperov MG, Bellenbaum N, et al (2013) IMILAST: A community
 676 effort to intercompare extratropical cyclone detection and tracking algo-
 677 rithms. Bulletin of the American Meteorological Society Bulletin of the
 678 American Meteorological Society 94:529–547. <https://doi.org/https://doi.org/10.1175/BAMS-D-11-00154.1>

680 Pall P, Aina T, Stone DA, et al (2011) Anthropogenic greenhouse gas contribu-
 681 tion to flood risk in england and wales in autumn 2000. Nature 470:382–385.
 682 <https://doi.org/10.1038/nature09762>

683 Philip S, Kew SF, van Oldenborgh GJ, et al (2018) Attribution analysis of the
 684 Ethiopian drought of 2015 p 2465–2486. <https://doi.org/https://doi.org/10.1175/JCLI-D-17-0274.1>

686 Pinto JG, Spanghel T, Ulbrich U, et al (2005) Sensitivities of a cyclone
 687 detection and tracking algorithm: individual tracks and climatology. Mete-
 688 orologische Zeitschrift 14(6):823–838. [https://doi.org/10.1127/0941-2948/
 689 2005/0068](https://doi.org/10.1127/0941-2948/2005/0068)

690 Priestley MDK, Catto JL (2022) Future changes in the extratropical storm
 691 tracks and cyclone intensity, wind speed, and structure. Weather and
 692 Climate Dynamics 3(1):337–360. <https://doi.org/10.5194/wcd-3-337-2022>

693 Pörtner HO, Roberts D, Poloczanska E, et al (2022) IPCC, 2022: Summary for
 694 policymakers. In: Climate Change 2022: Impacts, Adaptation, and Vulner-
 695 ability. Contribution of Working Group II to the Sixth Assessment Report
 696 of the Intergovernmental Panel on Climate Change

697 Reale M, Liberato ML, Lionello P, et al (2019) A global climatology of explosive
 698 cyclones using a multi-tracking approach. Tellus A: Dynamic Meteorology
 699 and Oceanography 71(1):1611,340. [https://doi.org/10.1080/16000870.2019.
 700 1611340](https://doi.org/10.1080/16000870.2019.1611340)

701 Riviera 24 (2021) A quattro mesi dalla tempesta Alex
 702 in Costa Azzurra si cercano ancora i corpi delle vit-
 703 time. Available at [https://www.riviera24.it/2021/02/
 704 a-quattro-mesi-dalla-tempesta-alex-in-costa-azzurra-si-cercano-ancora-i-corpi-delle-vit](https://www.riviera24.it/2021/02/a-quattro-mesi-dalla-tempesta-alex-in-costa-azzurra-si-cercano-ancora-i-corpi-delle-vit)
 705 Accessed: 07/01/2021

706 Sanders F, Gyakum JR (1980) Synoptic-dynamic climatology of the “bomb”.
 707 Monthly Weather Review 108:1589–1606. <https://doi.org/https://doi.org/>

10.1175/1520-0493(1980)108<1589:SDCOT>2.0.CO;2

Screen J, Simmonds I (2014) Amplified mid-latitude planetary waves favour particular regional weather extremes. *Nature Climate Change* 4:704–709. <https://doi.org/10.1038/nclimate2271>

Seneviratne S, Zhang X, Adnan M, et al (2021) Weather and climate extreme events in a changing climate. In *Climate Change 2021: The physical science basis. Contribution of Working Group I to the Sixth Assessment Report of the Intergovernmental Panel on Climate Change* [Masson-Delmotte, V., P. Zhai, A. Pirani, S.L. Connors, C. Péan, S. Berger, N. Caud, Y. Chen, L. Goldfarb, M.I. Gomis, M. Huang, K. Leitzell, E. Lonnoy, J.B.R. Matthews, T.K. Maycock, T. Waterfield, O. Yelekçi, R. Yu, and B. Zhou (eds.)]. Cambridge University Press. In Press.

Serreze MC, Barrett AP, Stroeve JC, et al (2009) The emergence of surface-based arctic amplification. *The Cryosphere* 3(1):11–19. <https://doi.org/10.5194/tc-3-11-2009>

Sinclair MR, Watterson IG (1999) Objective assessment of extratropical weather systems in simulated climates. *Journal of Climate* 12(12):3467–3485. [https://doi.org/10.1175/1520-0442\(1999\)012<3467:OAOEWS>2.0.CO;2](https://doi.org/10.1175/1520-0442(1999)012<3467:OAOEWS>2.0.CO;2)

Stott PA, Stone DA, Allen MR (2004) Human contribution to the European heatwave of 2003. *Nature* 432(7017):610–614. <https://doi.org/10.1038/Nature03089>

Stott PA, Christidis N, Otto FEL, et al (2016) Attribution of extreme weather and climate-related events. *Wiley Interdisciplinary Reviews: Climate Change* 7(1):23–41. <https://doi.org/10.1002/wcc.380>

Süveges M (2007) Likelihood estimation of the extremal index. *Extremes* 10(1–2):41–55. <https://doi.org/10.1063/1.5079656>, ISBN: 1386-1999 Publisher: Springer

The Watchers (2020) Death toll caused by storm Alex rises to 15, 21 still missing in France and Italy. Available at: <https://watchers.news/2020/10/07/storm-alex-death-toll-damage-october-2020/> Accessed: 07/02/2020

Tilinina N, Gulev SK, Rudeva I, et al (2013) Comparing cyclone life cycle characteristics and their interannual variability in different reanalyses. *Journal of Climate* 26:6419–6438

Vautard R, van Oldenborgh GJ, Otto FEL, et al (2019) Human influence on European winter wind storms such as those of January 2018. *Earth System Dynamics* 10(2):271–286. <https://doi.org/10.5194/esd-10-271-2019>

- 744 Wallace J, Lim G, Backmon M (1988) Relationship between cyclone tracks,
745 anticyclone tracks and baroclinic waveguides. *Journal of Atmospheric Sci-*
746 *ences* 45:439–462. [https://doi.org/https://doi.org/10.1175/1520-0469\(1988\)](https://doi.org/https://doi.org/10.1175/1520-0469(1988)045<0439:RBCTAT>2.0.CO;2)
747 [045<0439:RBCTAT>2.0.CO;2](https://doi.org/https://doi.org/10.1175/1520-0469(1988)045<0439:RBCTAT>2.0.CO;2)
- 748 Wilks D (2005) Chapter 5 – Hypothesis Testing. In: *Statistical Methods in the*
749 *Atmospheric Sciences*, 2nd edn.
- 750 WMO (1987) The measurement of gustiness at routine wind stations —
751 a review. Available at [https://library.wmo.int/doc_num.php?explnum_id=](https://library.wmo.int/doc_num.php?explnum_id=7372)
752 [7372](https://library.wmo.int/doc_num.php?explnum_id=7372)
- 753 WMO (2020) Mediterranean episode causes “unprecedented”
754 rainfall. Available at [https://public.wmo.int/en/media/news/](https://public.wmo.int/en/media/news/mediterranean-episode-causes-unprecedented-rainfall)
755 [mediterranean-episode-causes-unprecedented-rainfall](https://public.wmo.int/en/media/news/mediterranean-episode-causes-unprecedented-rainfall)
- 756 Yiou P (2014) Anawege: a weather generator based on analogues of atmo-
757 spheric circulation. *Geoscientific Model Development* 7(2):531–543. [https:](https://doi.org/10.5194/gmd-7-531-2014)
758 [//doi.org/10.5194/gmd-7-531-2014](https://doi.org/10.5194/gmd-7-531-2014)
- 759 Zappa G, Shaffrey LC, Hodges KI, et al (2013) A multimodel Assessment of
760 Future Projections of North Atlantic and European Extratropical Cyclones
761 in the CMIP5 Climate Models. *Journal of Climate* 26:5846–5862. [https:](https://doi.org/http://dx.doi.org/10.1175/JCLI-D-12-00573.1)
762 [//doi.org/http://dx.doi.org/10.1175/JCLI-D-12-00573.1](https://doi.org/http://dx.doi.org/10.1175/JCLI-D-12-00573.1)

763 **Appendix A Local dimension d and**

764 **persistence θ^{-1}**

765 Local dimension d is computed by applying extreme value statistics to Poincaré
766 recurrences of a state ζ (Lucarini et al, 2016). ζ , here represented by Alex’s
767 longitude-latitude sea-level pressure map, is a point in the phase space. The
768 trajectories in the phase space are successions of 6-hourly sea-level pressure
769 maps in a similar fashion as described in Faranda et al (2017). For the state
770 ζ , we compute the probability that the trajectory returns close to it, namely
771 within a ball of radius ϵ centered on ζ . This probability has been studied
772 first by Freitas et al (2008) and obeys an extreme value distribution. In order
773 to compute this probability, we first calculate the distances between ζ and
774 neighbourhood points within a radius ϵ as:

$$g(x(t)) = \log(\text{dist}(x(t), \zeta)) \quad (\text{A1})$$

775 where $\text{dist}(x(t), \zeta)$ is the Euclidean distance of SLP maps between each
776 timestep $x(t)$ and Alex (ζ). The Freitas-Freitas-Todd theorem (Freitas et al,
777 2008), modified by (Lucarini et al, 2012), states that the probability of recur-
778 rences, namely of $x(t)$ to fall inside a ball of radius ϵ and centered at ζ ,
779 converges to a Generalized Pareto Distribution:

$$P(z > s(q)) \simeq \exp\left[-\vartheta(\zeta) \frac{z - \mu(\zeta)}{\sigma(\zeta)}\right] \quad (\text{A2})$$

780 where $z = g(x(t))$. The radius ϵ is related to a threshold $s(q)$ of the time
 781 series of the distances computed as Eq. (A1), where the exceedances of the
 782 threshold are the points that fall within the radius ϵ from ζ . Therefore, the
 783 relation between ϵ and $s(q)$ is the following: $\epsilon = e^{-s(q)}$. In this work we compute
 784 $s(q)$ with q being the 99th percentile, so that 1% of the distances exceed the
 785 threshold (Fig. B9). The parameters μ and σ are obtained via fitting. $\mu(\zeta)$
 786 corresponds to the threshold $s(q)$, while the local dimension d is obtained as:
 787 $\sigma = 1/d(\zeta)$.

788 We fit a Generalized Pareto Distribution to the exceedances using the
 789 Maximum Likelihood estimator. We also have tested two other methods, the
 790 Method of Moments and L-moments, and we have found similar results, namely
 791 that when the differences between d in factual and counterfactual periods are
 792 statistically significant for a method, they also are so for the others (Fig. B10).

793 The extremal index θ is an adimensional parameter between 0 and 1 that
 794 can be interpreted as the inverse of the mean residence time. Hence, persistence
 795 is given by the inverse of θ . We compute θ using the [Süveges \(2007\)](#) estimator.

796 Appendix B Additional figures

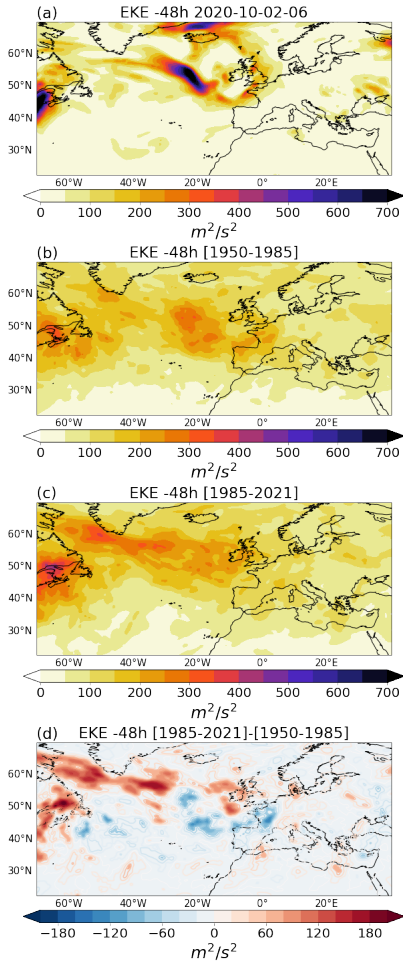


Fig. B1 Same as Fig. 2 (i-l) but for eddy kinetic energy centered 48 hours before Alex's lag 0 date (a) and analogue lag 0 dates (b-d).

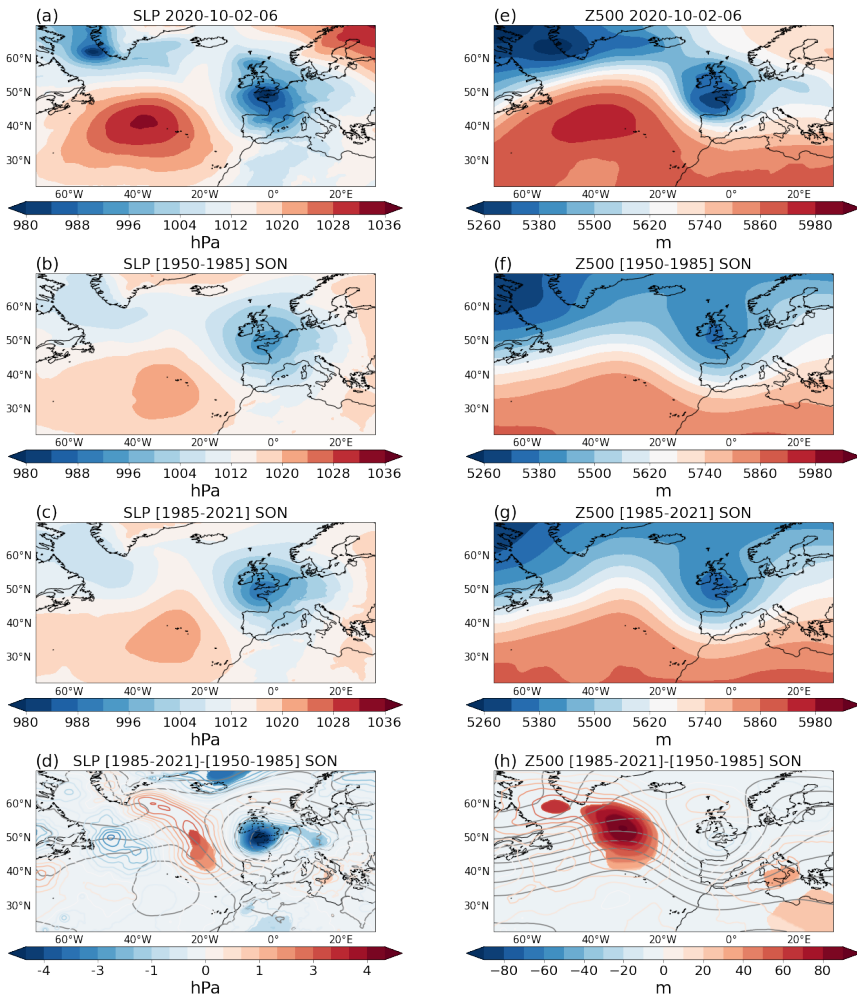


Fig. B2 Same as Fig. 2 (a-h) but for autumn (September-October-November) analogues

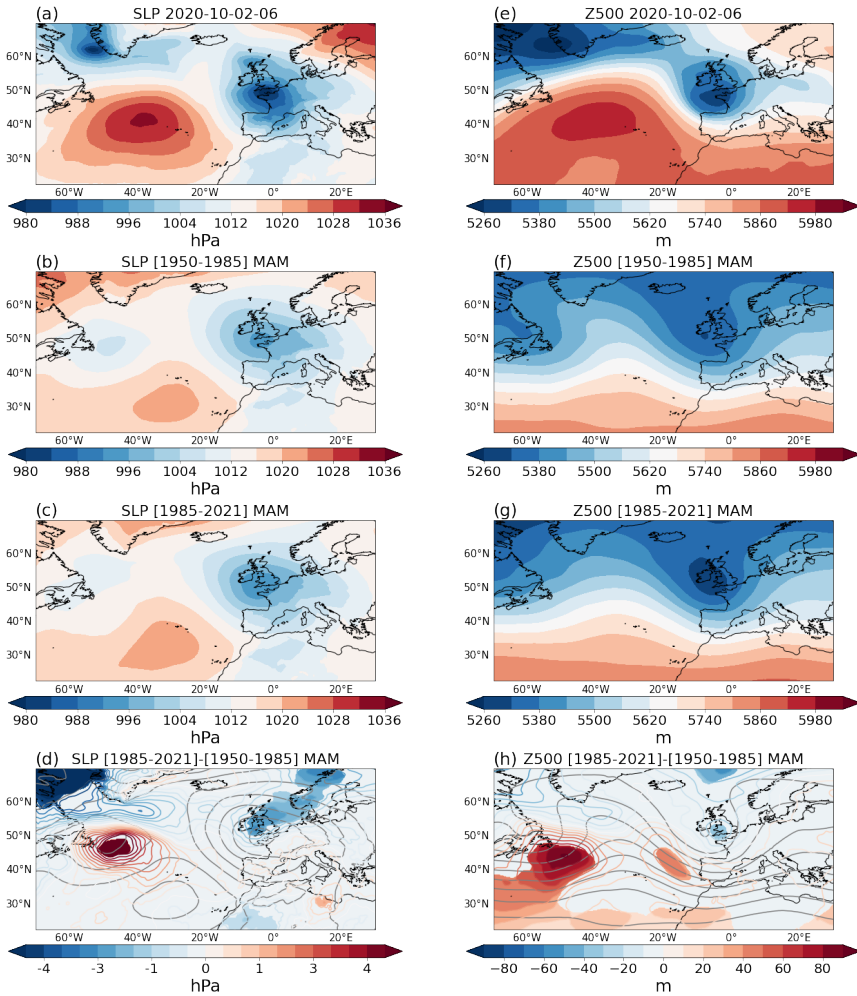


Fig. B3 Same as Fig. 2 (a–h) but for spring (March–April–May) analogues

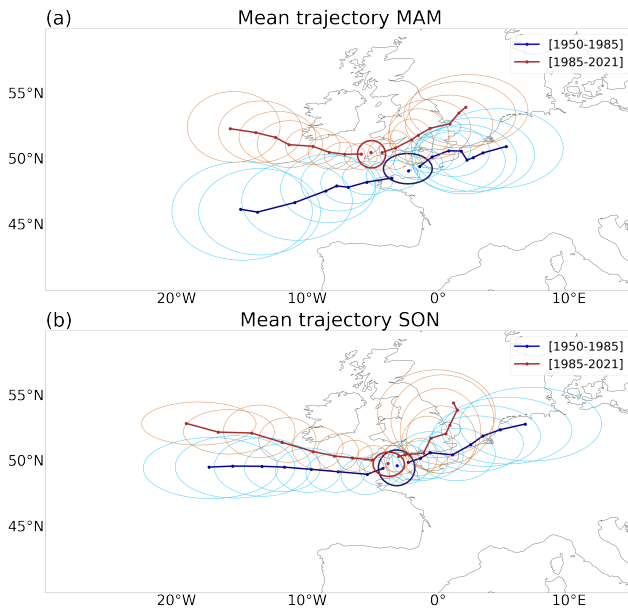


Fig. B4 Same as Fig. 4 but for (a) spring (March-April-May) analogues and (b) autumn (September-October-November) analogues.

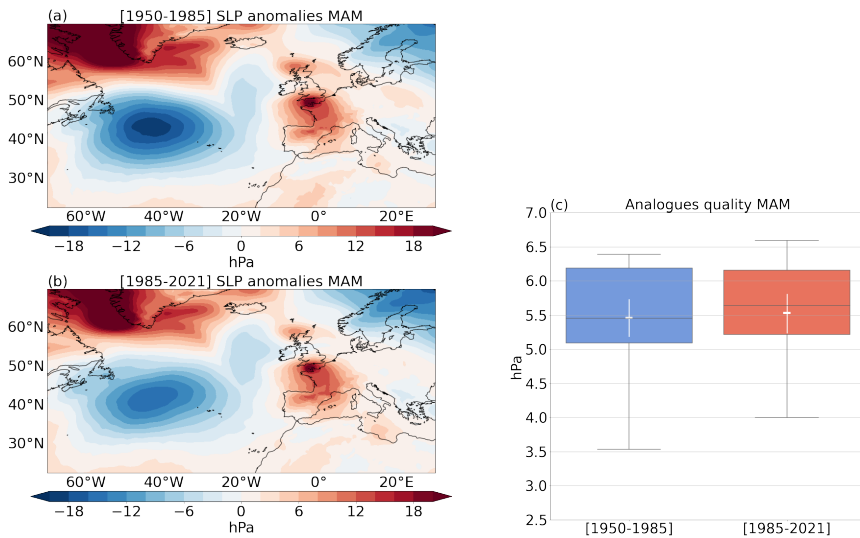


Fig. B5 Same as Fig. 6 but for spring (March-April-May) analogues

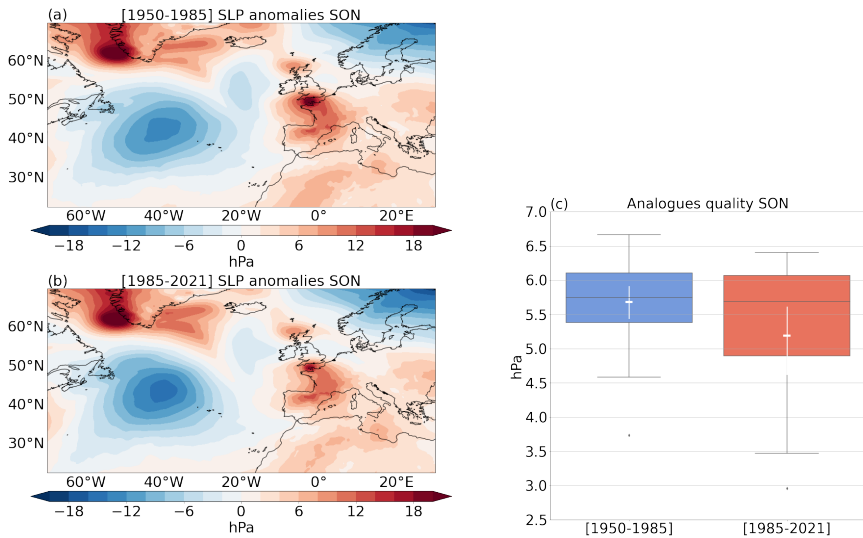


Fig. B6 Same as Fig. 6 (a–h) but for autumn (September–October–November) analogues

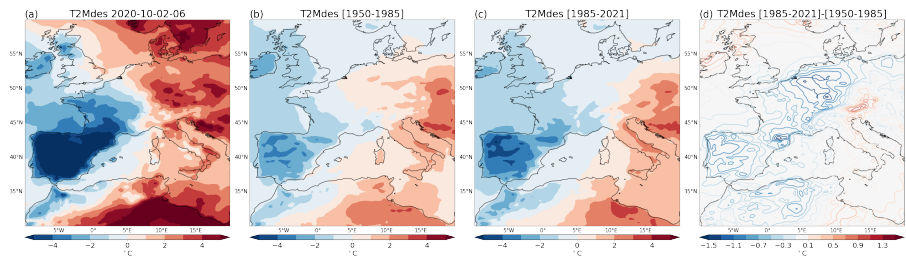


Fig. B7 24-hour means of deseasonalized 2-meter air temperature of Alex (a), counterfactual analogues (b), factual analogues (c) and differences between the two periods (d).

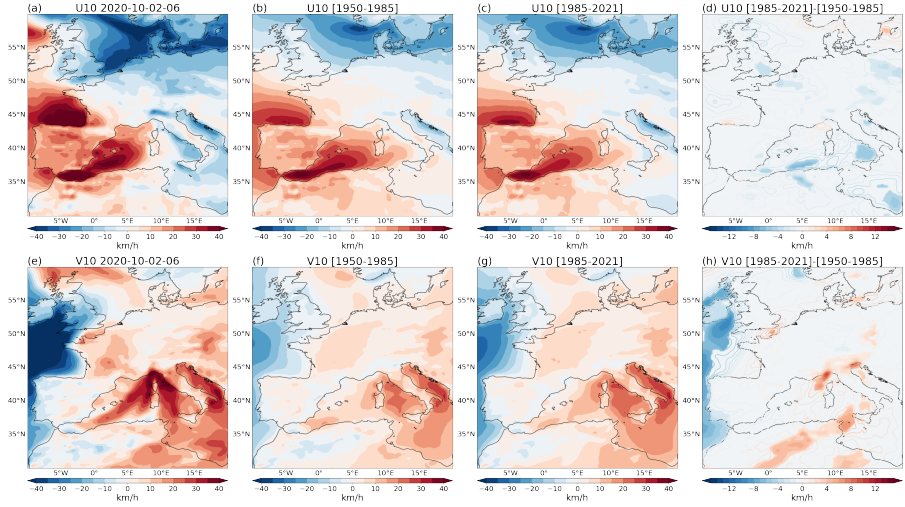


Fig. B8 24-hour means of 10m zonal wind (first row) and 10m meridional wind (second row) for Alex (a, e), counterfactual analogues (b,f), factual analogues (c,g), and difference between the two periods (d,h).

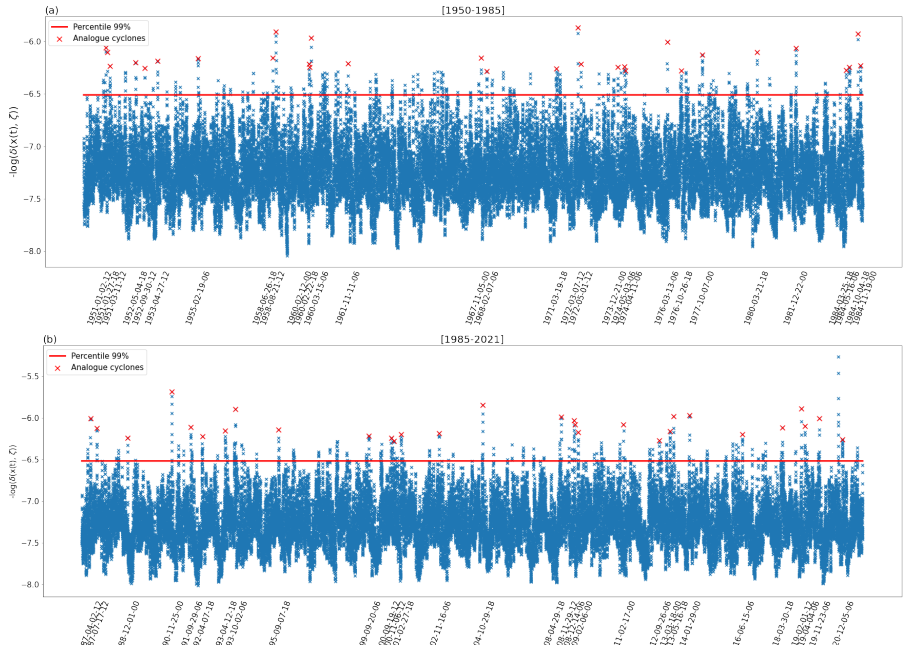


Fig. B9 Timeseries of the $\log(\text{dist}(x(t), \zeta))$ distances between Alex and the other timesteps for counterfactual (a) and factual (b) periods. Red crosses show the analogue cyclones. $\log \theta$ dates are indicated on the x-axis. Red lines show the 99% quantile, and the exceedances are used to compute the dynamical system metrics.

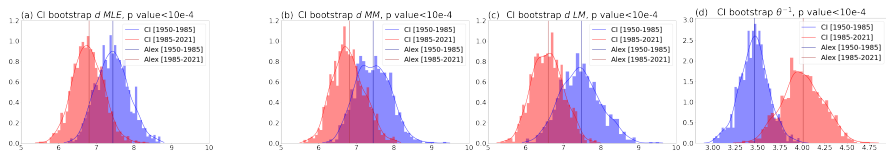


Fig. B10 Confidence interval using a bootstrap method for local dimension d computed using Maximum Likelihood Estimation (a), Method of Moments (b), and L-Moments (c), and for persistence θ^{-1} . The statistical significance of the difference of factual and counterfactual distributions has been assessed using the Kolmogorov-Smirnov test. P-values are shown in the panel titles.